[17]Brown, G. B., "The Mechanism of Edge-Tone Production," *Proceedings of the Physical Society*, Vol. 49, Pt. 5, 1937, pp. 508–521.
[18]Curle, N., "The Mechanics of Edge-Tones," *Proceedings of the Royal Society* A, Vol. 216, 1953, pp. 412–424.
[19]Ern, P., "Etude Expérimentale d'un Jet Confiné," Rapport de Diplôme d'Etudes Approfondies, Université Paris XI, Paris, France, June 1994.

Kármán Vortex Development: Relation to Symmetry and Circulation of Transition Vortices

C.-K. Chyu* and D. Rockwell†
Lehigh University, Bethlehem, Pennsylvania 18055

Introduction

At sufficiently high Reynolds number, the shear layers separating from a cylinder exhibit well-defined, small-scale concentrations of vorticity that feed into the large-scale Kármán vortices. Bloor[1] and Gerrard[2] characterized various features of these small-scale structures and their consequence on the mean flow features of the near wake. This Bloor–Gerrard mechanism of transition is, for the range of Reynolds numbers of interest herein, essentially due to amplification of a thin shear-layer instability. Its overall character is that of a Kelvin–Helmholtz instability, but it is more explicitly described as a solution of the Rayleigh equation. The principal features of the small-scale shear-layer vortices, from both quasi-two-dimensional and three-dimensional perspectives, have been assessed.[3–11] The inherent instability frequency of these vortices and their control by application of external disturbances are clearly established in several of these investigations.

The issue arises as to how the rate of development and the symmetry of (i.e., phase shift between) small-scale vortices in opposing shear layers influence the location and form of the large-scale Kármán vortices formed in the near wake. Indeed, the shear-layer vortices do, in the end, comprise the Kármán vortices. These features are investigated using instantaneous images of vorticity.

Experimental System and Techniques

Experiments were carried out in a free-surface water channel. It had a square test section of 597×597 mm and a length of 4000 mm. The water level was maintained at a height of approximately 530 mm. A cylinder of diameter $D = 25.4$ mm was mounted horizontally at the middepth of the water channel; a vertical false wall isolated the cylinder support from the main flow through the test section. Details of this experimental arrangement are given by Chyu.[12] The freestream velocity was maintained at $U = 182$ mm/s, giving a value of Reynolds number of $Re = 5 \times 10^3$.

The instantaneous velocity field over the entire midplane of the cylinder was determined using a laser-scanning version of high-image-density particle image velocimetry (PIV). This approach is described by Rockwell et al.[13,14] and Rockwell and Lin.[15] The laser-scanning system involves an argon-ion (4-W) laser, which was deflected from a rotating mirror with 72 facets. The flow was seeded with 12-μm-diam hollow glass spheres coated with a thin layer of silver. Particle images were recorded on high-resolution 35-mm film via a Nikon F4 camera with a 105-mm lens. The lens system has a magnification factor $M = 1{:}2.9$. Directional ambiguity was avoided by employing a bias mirror immediately in front of the camera lens. The 35-mm negatives were digitized at a high resolution of 125 pixels/mm, then interrogated at a window size 100×100 pixels with 50% overlap. The velocity vector corresponding to each interrogation window was obtained using a single-frame cross-correlation approach. The grid in the plane of the laser sheet had a spacing of 1.63 mm. The estimated uncertainties of the velocity and vorticity are approximately 0.5 and 4%, respectively.

Instantaneous and Averaged Vorticity Distributions and Streamline Patterns

Figure 1 shows images of vorticity distributions at instants of time 1, 2, and 3. The instantaneous images, which were acquired at a time interval corresponding to the period of Kármán vortex formation, are representative of the extreme states of the wake. The image of averaged vorticity was obtained from an ensemble average of the three instantaneous images. The intent of this averaged image is to demonstrate the lack of phase locking of the small-scale, shear-layer vortices during formation of successive Kármán vortices for a limited number of Kármán cycles. The blank region on the upper side of the cylinder is due to the shadow of the laser sheet in that region. The small-scale concentrations of vorticity represent the manifestations of the transition first identified by Bloor[1] and Gerrard.[2] The shear-layer vortices eventually agglomerate to form the large-scale Kármán vortex, indicated by the negative (bold white) region of vorticity extending across the entire wake in each of the three instantaneous images. At instant 1, a sequence of small-scale vortices, as many as three to five, are clearly evident in the upper and lower shear layers from the cylinder. The Kármán vortex has approximately an elliptical shape, and its major axis is oriented vertically. At instant 2, however, the development of the pattern of shear-layer vortices is not as consistent; in fact, there is an abrupt appearance of a relatively large-scale vortex in the upper shear layer. This development of the shear-layer system is associated with a Kármán vortex that is inclined at an angle of about 45 deg but still extends across the entire wake. Finally, the development of the shear-layer vortices at instant 3 occurs rapidly and in phase in both the upper and lower shear layers. That is, at a given streamwise location, the location and scale of the first three vortices are nearly mirror images of each other in the opposite shear layers. Moreover, the vorticity contour levels suggest that the second shear-layer vortices have rapidly attained a large value of circulation, relative to their counterparts in image 1. In this case, the Kármán vortex on the lower side forms relatively late and is inclined at a shallow angle, relative to instants 1 and 2. These three instantaneous images are representative of the extreme states of the wake over many Kármán cycles. The sequence of patterns shown in these images is, however, not generally repeatable.

The averaged image reveals that the detailed, instantaneous structure of the shear-layer vortices is essentially lost. Indications of the rate of development and phase between these small-scale concentrations of vorticity on opposite sides of the wake, so evident in images 1, 2, and 3, are not apparent in the averaged image. Moreover, inspection of the averaged contours of the Kármán vortex shows low levels, and therefore a small value of total circulation, relative to each of the instantaneous representations of the Kármán vortex. This is because the centroids of each of the instantaneous Kármán concentrations generally occur at markedly different locations in the instantaneous images, i.e., they are not phase locked to the Kármán formation.

Figure 2 gives values of circulation of the vortices for the instantaneous and averaged images. Rectangular boxes indicate the circuits employed for evaluation of the circulation $\Gamma^* = \Gamma/\pi U D$, in which Γ is circulation, U is freestream velocity and D is cylinder diameter. Viewing, first of all, the values of Γ^* for the shear-layer vortices, they typically have an initial value on the order of 0.1, but more mature concentrations show levels as high as the order of 0.2. The magnitude of Γ^* of the shear-layer vortices relative to the eventually formed Kármán vortices is of interest. In an attempt to establish this relationship, an approximate circuit is drawn around the large-scale agglomeration of image 1. It has a value of 0.79. We conclude that the vortices formed in the shear layer of image 1

Received May 11, 1995; revision received Sept. 22, 1995; accepted for publication Oct. 7, 1995.

*Research Assistant, Department of Mechanical Engineering and Mechanics, 19 Memorial Drive West.
†Paul B. Reinhold Professor, Department of Mechanical Engineering and Mechanics, 354 Packard Laboratory, 19 Memorial Drive West. Member AIAA.

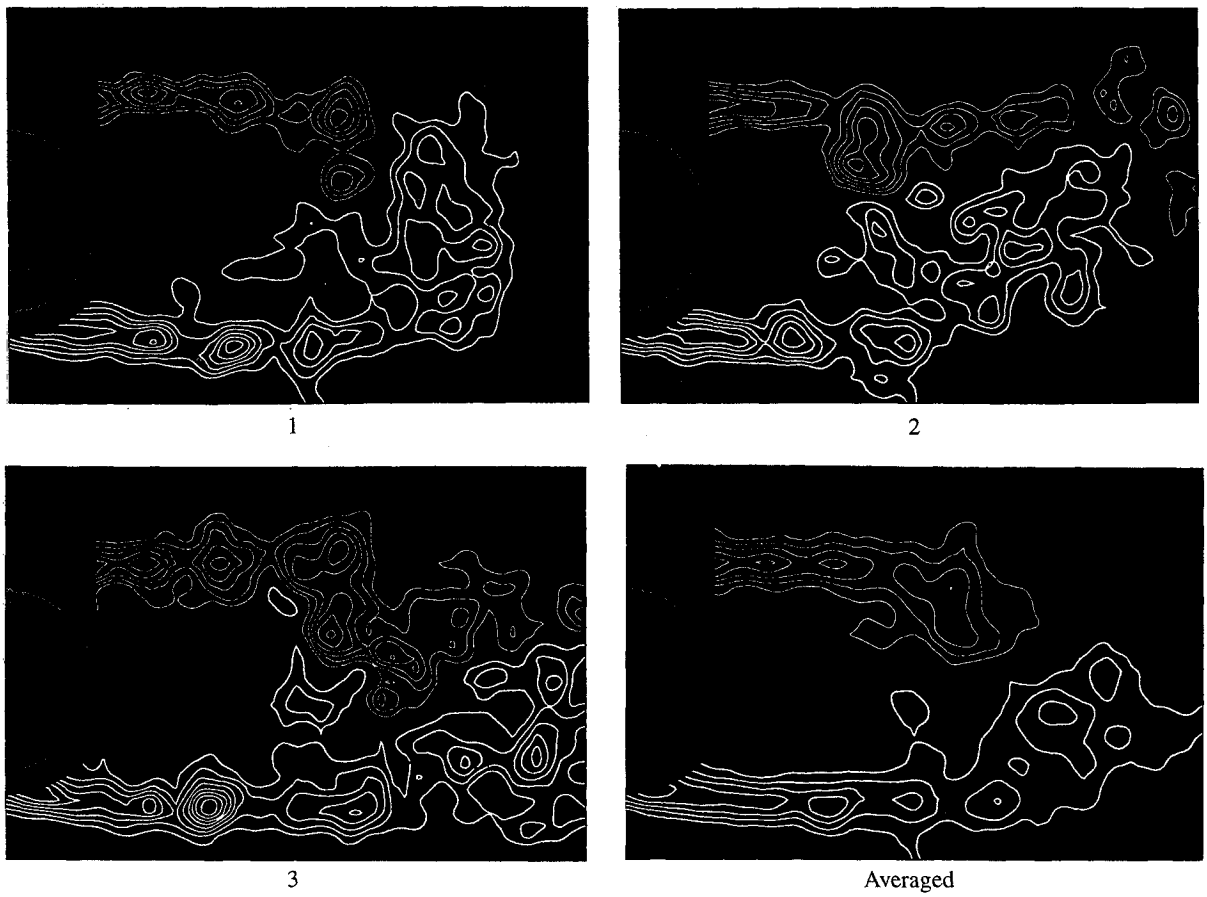

Fig. 1 Instantaneous and averaged near-wake vorticity fields for $Re = 5 \times 10^3$. Minimum contour level $|\omega_{min}| = 10\ s^{-1}$ and contour increment $\Delta\omega = 10\ s^{-1}$.

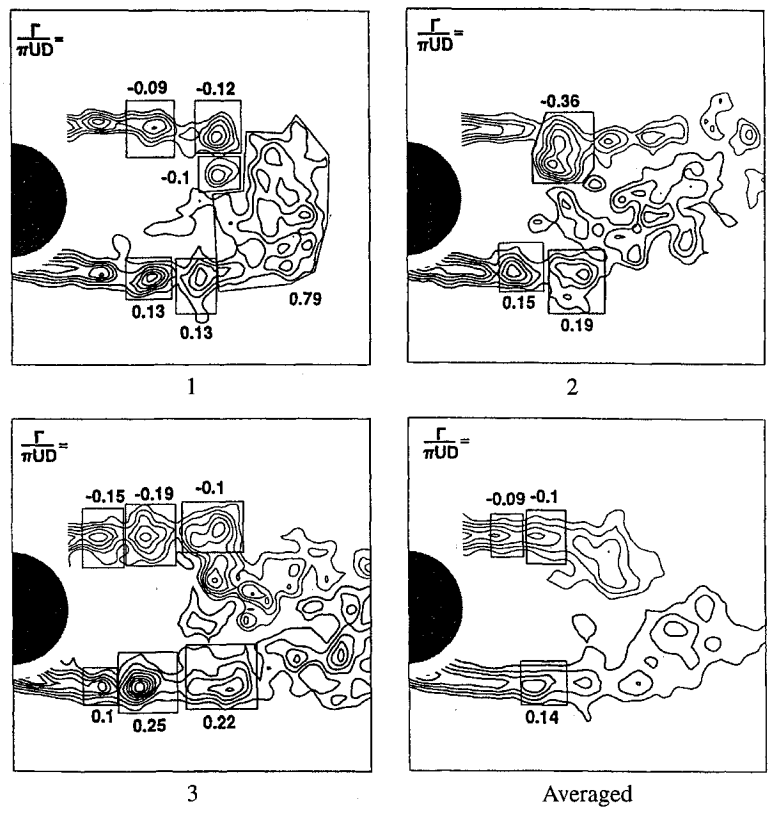

Fig. 2 Dimensionless circulation $\Gamma/\pi UD$ of shear-layer and Kármán vortices. Minimum vorticity contour level $|\omega_{min}| = 10\ s^{-1}$ and contour increment $\Delta\omega = 10\ s^{-1}$.

can have an approximate value of Γ^* as high as approximately one-eighth that of the Kármán vortices. This ratio is likely higher for image 3, where the shear-layer vortices attain larger values of Γ^*.

Conclusions

Over a range of Reynolds number represented by $Re = 5 \times 10^3$, the Kármán vortices form relatively far downstream of the cylinder. Moreover, the small-scale, shear-layer vortices formed immediately downstream of separation exhibit different rates of development and symmetry from cycle to cycle of the Kármán vortex formation. In turn, the nature of the shear-layer vortex system is linked to the location and orientation of the eventually formed Kármán vortex. When the vortices develop symmetrically in the opposing shear layers, and quickly attain relatively large values of circulation, the Kármán vortex is formed further downstream.

The instantaneous circulation of the vortices can reach a value as large as one-eighth that of the Kármán vortex. Attempts to deduce this circulation, using phase-referenced measurements triggered on the Kármán vortex, are not meaningful because the shear-layer vortices are not phase locked to the Kármán vortices.

Further efforts should address the spanwise correlation of the shear-layer and Kármán vortex development to determine the degree to which the foregoing observations are influenced by three-dimensional distortions.

Acknowledgments

The authors gratefully acknowledge the financial support of the Office of Naval Research through Grants N00014-94-1-0185 and N00014-90-J-1510, monitored by Thomas Swean.

References

[1]Bloor, M. S., "The Transition to Turbulence in the Wake of a Circular Cylinder," *Journal of Fluid Mechanics*, Vol. 19, Pt. 2, 1964, pp. 290–319.

[2]Gerrard, J. H., "A Disturbance-Sensitive Reynolds Number Range of Flow Past a Circular Cylinder," *Journal of Fluid Mechanics*, Vol. 22, Pt. 1, 1965, pp. 187–196.

[3]Gerrard, J. H., "The Wakes of a Cylindrical Bluff Body at Low Reynolds Number," *Philosophical Transactions of the Royal Society of London, Series A: Mathematical and Physical Sciences*, Vol. 288, 1978, pp. 351–382.

[4]Wei, T., and Smith, C. R., "Secondary Vortices in the Wake of Circular Cylinders," *Journal of Fluid Mechanics*, Vol. 169, Aug. 1986, pp. 513–533.

[5]Kourta, A., Boisson, H. C., Chassing, P., and Haminh, H., "Nonlinear Interaction and the Transition to Turbulence in the Wake of a Circular Cylinder," *Journal of Fluid Mechanics*, Vol. 181, Aug. 1987, pp. 141–161.

[6]Unal, M. F., and Rockwell, D., "On Vortex Formation from a Cylinder. Part 1. The Initial Instability," *Journal of Fluid Mechanics*, Vol. 190, May 1988, pp. 491–512.

[7]Filler, J. R., Marston, P. L., and Mieh, W. C., "Response of the Shear Layer Separating from a Circular Cylinder to Small-Amplitude Rotational Oscillations," *Journal of Fluid Mechanics*, Vol. 231, Oct. 1991, pp. 481–499.

[8]Ahmed, A., Khan, M. J., and Bays-Muchmore, B., "Experimental Investigation of a Three-Dimensional Bluff-Body Wake," *AIAA Journal*, Vol. 31, No. 3, 1993, pp. 559–563.

[9]Sheridan, J., Soria, J., Wu, J., and Welsh, M. C., "The Kelvin–Helmholtz Instability of the Separated Shear Layer from a Circular Cylinder," *Bluff-Body Wakes, Dynamics and Instabilities*, edited by H. Eckelmann, J. M. Graham, P. Huerre, and P. A. Monkewitz, Proceedings of IUTAM Symposium (Goettingen, Germany, Sept. 1992), Springer–Verlag, Berlin, 1993, pp. 115–117.

[10]Chyu, C.-K., Lin, J.-C., Sheridan, J., and Rockwell, D., "Kármán Vortex Formation from a Cylinder: Role of Phase-Locked Kelvin–Helmholtz Vortices," *Physics of Fluids*, Vol. 7, No. 9, 1995, pp. 2288–2290.

[11]Lin, J.-C., Towfighi, J., and Rockwell, D., "Instantaneous Structure of Near-Wake of a Circular Cylinder: On the Effect of Reynolds Number," *Journal of Fluids and Structures*, Vol. 9, 1995, pp. 659–669.

[12]Chyu, C.-K., "A Study of the Near-Wake Structure from a Circular Cylinder," Ph.D. Dissertation, Dept. of Mechanical Engineering and Mechanics, Lehigh Univ., Bethlehem, PA, 1995.

[13]Rockwell, D., Towfighi, J., Magness, C., Akin, O., Corcoran, T., Robinson, O., and Gu, W., "Instantaneous Structure of Unsteady Separated Flows via Particle Image Velocimetry," Fluid Mechanics Labs., Dept. of Mechanical Engineering and Mechanics, Lehigh Univ., Rept. PI-1, Bethlehem, PA, Feb. 1992.

[14]Rockwell, D., Magness, C., Towfighi, J., Akin, O., and Corcoran, T., "High-Image-Density Particle Image Velocimetry Using Laser Scanning Techniques," *Experiments in Fluids*, Vol. 14, No. 3, 1993, pp. 181–192.

[15]Rockwell, D., and Lin, J.-C., "Quantitative Interpretation of Complex, Unsteady Flows via High Image-Density Particle Image Velocimetry," *Optical Diagnostics in Fluid and Thermal Flow*, Proceedings of SPIE, The International Society for Optical Engineering, Vol. 2005, Bellingham, WA, 1993, pp. 490–503.

Correlation of Shock Angles Caused by Flat Delta Wings

S. Koide*
Japan Defense Agency, Tokyo 190, Japan

Introduction

FOR the glancing shock-wave/turbulent-boundary-layer interactions, the inviscid shock wave has an important role for specifying the interaction behavior regardless of the shape of the shock generator. Hence, the trace of the shock wave on the wall provides an important reference position (the imaginary position that would exist if no boundary layer were presented on the wall) for understanding the interaction. The author recently proposed a correlation law for the shock angles caused by a series of rhombic delta wings (RDWs).[1] Using the correlation law, the shock angle on the plane of symmetry of the wing, β, can be predicted easily for a wide range of wing geometries (specified by half-apex angle α and sweep angle λ) and flow Mach numbers M (see Fig. 1a). This angle specifies the trace of shock wave on the wall when a sharp fin, whose cross section is a triangle (the half-cut model of the RDW; see Fig. 1a), is placed on a wall (equivalent to the position of the plane of symmetry for the wing). In this Note, the correlation law is expanded for the delta wings (FDWs). Using the expanded law, the trace of the shock generated by a swept sharp fin can be specified on the wall for various α (angle of attack), λ, and M (see Fig. 1b). The difference of the shock angles caused by the two disparate wings, the RDW and the FDW, is also discussed.

Correlation of the Shock Angles

Unlike the case of the RDWs,[1] several data are available for the FDW shock angles. They have been obtained experimentally by Deng et al.[2] for $6 \leqq \alpha \leqq 20$ deg and $\lambda = 15$ and 50 deg at $M = 2.04$, Fomison and Stollery[3] for $6.5 \leqq \alpha \leqq 35$ deg and $30 \leqq \lambda \leqq 75$ deg at $M = 2.40$, Settles and Lu[4] for $5 \leqq \alpha \leqq 15$ deg and $10 \leqq \lambda \leqq 65$ deg at $M = 2.95$, and computationally by Klunker et al.[5] for $\alpha = 15$ deg and $\lambda = 50$ deg at $M = 4.0$. Based on these data, a correlation of β with M, α, and λ has been considered.

To construct the correlation law for the RDWs, the angle between the plane of symmetry and the face of the delta wing,

$$\xi = \tan^{-1}[1/(\sin\alpha \cdot \tan\lambda)] \tag{1}$$

(see Fig. 1a), was employed. The value expressed by Eq. (1) corresponds to the angle ξ shown in Fig. 1b for the case of the FDWs. By introducing ξ, it is convenient that the two variables α and λ are represented by the single parameter. In the same way for the RDWs, ξ tends to depart from 90 deg when α and λ increase. Similarly β will decrease from its value at $\lambda = 0$ deg (i.e., the oblique shock angle for an unswept sharp fin of half-wedge angle α, expressed by β_{os}) as ξ drops below 90 deg. Hence, it was believed that the angle ξ could be suitable also for correlating the shock angles of the FDWs. As a matter of fact, the same parameter used for the RDWs,

$$(\beta/\beta_{os}) \cdot 2\xi/(\pi M^a) \tag{2}$$

Received Aug. 16, 1995; revision received Nov. 22, 1995; accepted for publication Nov. 30, 1995.

*Senior Research Engineer, 2–5th Laboratory, 3rd Research Center, 1-2-10 Sakae, Tachikawa. Member AIAA.